

# Phase Shift Keying on the Hypersphere: Power-Efficient MIMO Communications

Christoph Rachinger, Ralf R. Müller and Johannes B. Huber  
 Friedrich-Alexander-University Erlangen-Nürnberg, Germany  
 Email: {christoph.rachinger, ralf.r.mueller, johannes.huber}@fau.de

**Abstract**—We present Phase Shift Keying on the Hypersphere (PSKH), a generalization of conventional Phase Shift Keying (PSK) for Multiple-Input Multiple-Output (MIMO) systems, where data constellations are distributed over a multidimensional hypersphere. The use of such constellations with Peak-To-Average-Sum-Power-Ratio (PASPR) of 1 allows to use load-modulated transmitter which require a much smaller backoff, which in turn results in reduced power loss. In this paper we discuss several methods how to generate PSKH constellations and compare their performance. Bandwidth and power efficiency of PSKH systems can be greatly influenced by the choice of different pulse shapes which affect spectrum and PASPR of the transmission system. In order to further reduce the PASPR of our transmission signal, we use spherical interpolation to generate a smooth signal over the hypersphere and present the corresponding receiver and how complexity-reduction techniques influence the system performance. Finally, we discuss the methods presented in this paper regarding their trade-offs with respect to PASPR, spectrum, power efficiency and receiver complexity.

**Index Terms**—Multiple-input multiple-output systems, wireless communications, peak-to-average-power, load-modulation.

## I. INTRODUCTION

POWER efficiency has been one of the driving forces behind the development of current communication technologies. Unfortunately, one of the main sources of power consumption are amplifiers operated at low power efficiency. This holds even for state-of-the-art amplifiers, which cannot be operated at their optimal power level, because signals with suboptimal Peak-To-Average-Power-Ratio (PAPR), i.e. a  $\text{PAPR} > 1$ , require a certain backoff of the amplifier to avoid clipping. Constant envelope modulation schemes such as continuous phase modulation (CPM) provide an optimal PAPR and reduce the backoff compared to other modulation schemes, such as the widely used QAM [1]. While this improves the power efficiency of a transmission system, the bandwidth efficiency suffers: Since the radius in the complex plane is fixed for constant envelope transmission, phase remains the only degree of freedom to modulate information. This results in a rate loss compared to QAM, which is why constant envelope modulation did not receive much attention in the last years.

The use of MIMO systems allows for another method to increase power efficiency: Not the PAPR, but the Peak-to-Average-Sum-Power-Ratio (PASPR) of a vector-valued signal can be the deciding factor. This quantity is defined as

$$\text{PASPR}(\mathbf{x}(t)) = \frac{\max_t \|\mathbf{x}(t)\|^2}{\mathcal{E}\{\|\mathbf{x}(t)\|^2\}}. \quad (1)$$

Using the PASPR as a decisive factor is made possible by the use of recently developed load-modulated MIMO amplifiers [2], [3]. Since the degrees of freedom are reduced by only one for all antennas, the rate loss becomes smaller as more antennas are used [4]. For massive MIMO systems, the central limit theorem (CTL) guarantees that the PASPR becomes optimal as long as the data points are distributed on a multidimensional hypersphere. We call these constellations *Phase Shift Keying on the Hypersphere* (PSKH), because it is a natural extension of ordinary PSK. In conventional MIMO with only a handful of antennas, large fluctuations are still possible and therefore the PASPR is far from optimal. Thus some more adaptations are necessary in order to reduce the PASPR of the transmission signal.

The rest of this paper is organized as follows: In Sec. II we introduce our system model. Unlike in PSK, there are multiple ways to construct a constellation. Thus we discuss some algorithms to generate PSKH constellations and their advantages and disadvantages in Sec. III. Sec. IV deals with PASPR reduction of the output signal and how these techniques affect the spectrum. Secs. V and VI presents two of these approaches in more detail. This includes receiver structures for the corresponding signals as well as numerical results on the performance of them. The paper ends with a conclusion in Sec. VII.

## II. SYSTEM MODEL

For our work we assume transmission over the standard discrete time MIMO channel

$$\mathbf{y}[k] = \mathbf{H}\mathbf{x}[k] + \mathbf{n}[k] \quad (2)$$

where  $\mathbf{x}[k] \in \mathbb{C}^{n_T}$ ,  $\mathbf{y}[k] \in \mathbb{C}^{n_R}$  are transmit and receive vector at time  $k$ , respectively,  $\mathbf{H} \in \mathbb{C}^{n_T \times n_R}$  is the channel matrix and  $\mathbf{n}[k] \in \mathbb{C}^{n_R}$  is complex i.i.d. additive white Gaussian noise with variance  $\sigma^2$  per component.  $n_R$  and  $n_T$  denote the number of transmit and receive antennas respectively, but for the remainder of this paper we assume that  $n = n_R = n_T$  and omit the time index  $k$  unless confusion is possible. This model implicitly assumes that  $\sqrt{N}$  Nyquist-pulse shapes with optimal matched filters are used. If other pulse shaping filters are used, we will point it out.

The channel signal-to-noise-ratio is given as

$$\text{SNR} = \frac{\mathcal{E}\{\|\mathbf{x}\|^2\}}{\mathcal{E}\{\|\mathbf{n}\|^2\}} = \frac{P}{n\sigma^2} \quad (3)$$

where  $\sqrt{P}$  defines the radius of the PSKH constellation (see Sec. III). If the entries of  $\mathbf{H}$  are i.i.d complex Gaussian random variables with unit variance, the average received energy per information bit over the noise-spectral density is given as

$$\frac{E_b}{N_0} = \frac{nP}{R_m \sigma^2} \quad (4)$$

with  $R_m$  being the modulation rate.

### III. PSKH CONSTELLATIONS

#### A. Constellation Construction

We define a PSKH constellations as a set of  $M = 2^{R_m}$  data points  $\mathcal{A} = \{\mathbf{a}_0, \dots, \mathbf{a}_{M-1} \mid \mathbf{a}_i \in \mathbb{C}^n, \|\mathbf{a}_i\| = \sqrt{P}\}$ . Here,  $R_m$  is the number of binary symbols represented by one data point and  $P$  is the signal power. The vectors  $\mathbf{a}_i \in \mathbb{C}^n$  are  $n$ -dimensional corresponding to  $n$  transmit antennas in a MIMO system. We note that our PSKH constellations are also known as *spherical codes* in literature, but to our knowledge they have never been used to improve power efficiency of communication systems. Without further restrictions than the radius, there are many possible ways to create constellations, which might differ quite vastly in terms of quality. A reasonable measure for quality, as in all PAM schemes, is the minimum distance between signal points. Optimal codes in this sense and their analytic description, however, are known only for some restricted constellation sizes and dimensions [5].<sup>1</sup> Because of this we compare four different algorithms to generate PSKH constellations:

- *Equal Area Partitioning* (EQPA) from [7]: Generates a constellation with equally sized areas, which are usually not the Voronoi regions of a data point.
- *k-means Clustering* (kMC) using the spherical k-means algorithm [8]: Generates a large number of uniformly distributed points on the sphere, clusters them using the spherical k-means algorithm.
- *Potential Minimization* (PM): Generates particles on a sphere and minimize their potential energy. This can be done via a molecular dynamics simulation [9].
- *Per-Antenna PSK* (PA-PSK): Generates independent PSK constellations on each antenna, then scales them to fit the power constraint.

The algorithms can be distinguished in terms of construction complexity: EQPA and PA-PSK are analytic constructions, kMC and PM rely on numerical methods and are therefore more expensive to construct. Of course, such a construction needs to be done only once and can be computed offline. If construction is nonanalytic, it is further necessary to store the constellation in memory, which we think is reasonable to implement for  $R_m \lesssim 10$ . Otherwise it is possible to construct a constellation for only half the antennas and duplicate it, which results in a small degradation of quality.

In order to compare constellations with respect to their performance, we take a look at three different properties: Constellation-constrained capacities, minimum distance of the constellation (also known as *packing radius* in the context of spherical codes and packings) and error probabilities, i.e., bandwidth efficiency.

<sup>1</sup>Some examples of such optimal packings can be found in [6].

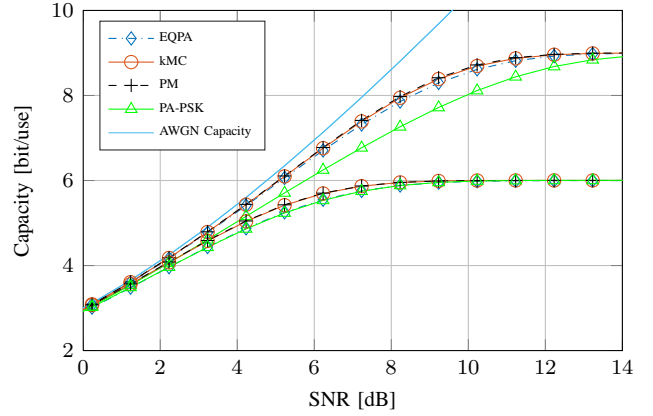


Fig. 1. Capacity of different constellations for a constellation sizes  $M = 64$  and  $M = 512$  points and  $n = 3$  antennas.

#### B. Capacity of PSKH

For continuous input, uniform distribution on the hyper-sphere is capacity achieving if  $\mathbf{H}$  is unitary [4]. In this section, we compare the capacities if the input is discrete and constrained to a certain size and  $\mathbf{H}$  is unitary. In Fig. 1 we plot the constellation constrained capacities for  $n = 3$  antennas and  $M = 64$  as well as  $M = 512$  points. As a baseline, we also plot the AWGN capacity  $C = \frac{1}{2} \log(1 + \text{SNR})$  (adapted to the number of antennas). The results are similar for different constellation and antenna array sizes, which is why we omit them here. The general result from these capacities can be explained as summarized: PM and kMC have the best capacities with PM outperforming kMC by only approx. 0.01 dB. If we want to transmit 1 bit per real dimension, PA-PSK and EQPA lose up to 0.5 dB at a capacity of  $C = 5$  bit/use. If we increase the constellation size, PM and kMC still remain on top, EQPA reduces the loss to about 0.3 dB, whereas PA-PSK loses 1.6 dB compared to PM at  $C = 8$  bit/use. The reason for this big loss when increasing the constellation size is that PA-PSK is the only constellation where no form of global optimization takes place. While a PSK constellation might be perfect on an individual antenna, increasing the total constellation size requires to use different PSK constellations on each antenna. This can have devastating influence on the overall distance properties of the constellation. On the other hand, EQPA works in such a way that the distribution of points becomes more and more uniform as the constellation size increases.

#### C. Distance Properties and BER Performance

In order to compare the distance properties of the individual algorithms, Table I lists the *total* and *average minimum distance* of a constellation defined as

$$d_{\min, \text{tot}}(\mathcal{A}) = \min_{\substack{\mathbf{a}_i, \mathbf{a}_j \in \mathcal{A} \\ i \neq j}} \|\mathbf{a}_i - \mathbf{a}_j\| \quad (5)$$

and

$$d_{\min, \text{avg}}(\mathcal{A}) = \mathcal{E}_{\mathbf{a}} \left\{ \min_{\substack{\mathbf{a} \in \mathcal{A} \\ \hat{\mathbf{a}} \neq \mathbf{a}}} \|\mathbf{a} - \hat{\mathbf{a}}\| \right\}. \quad (6)$$

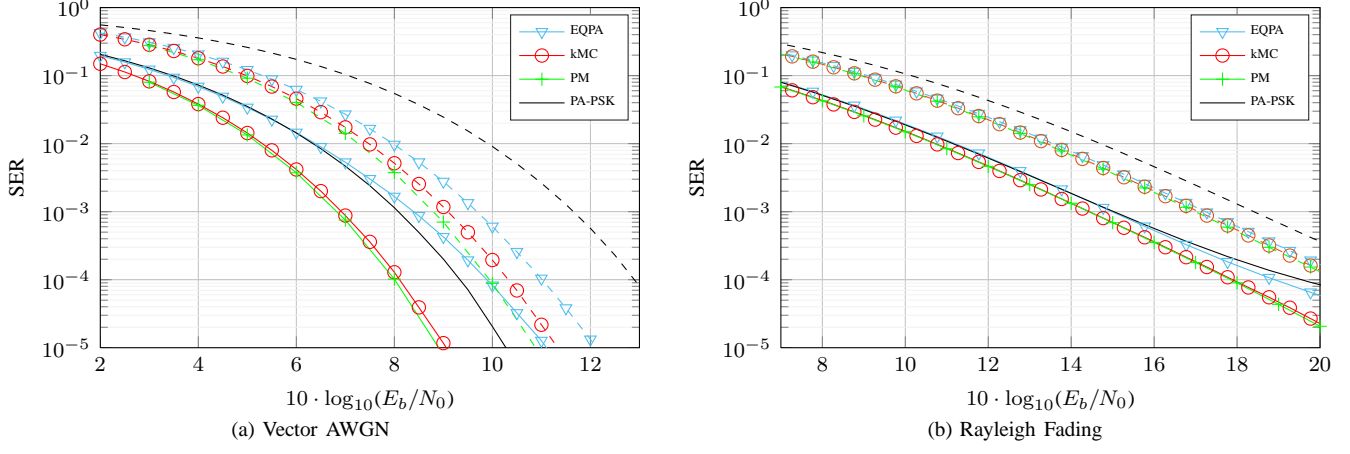


Fig. 2. Symbol error rate (SER) for transmission of  $R_m = 6$  (solid) or  $R_m = 9$  (dashed) bits per constellation point over a vector AWGN channel or a Rayleigh fading channel. The system has  $n = 3$  antennas.

TABLE I  
AVERAGE AND TOTAL MINIMUM DISTANCE OF CONSTELLATIONS

	$d_{\min, \text{tot}}$	$d_{\min, \text{avg}}$
EQPA, $M = 64$	0.6611	0.7282
kMC, $M = 64$	0.8674	0.9207
PM, $M = 64$	0.9139	0.9474
PA-PSK, $M = 64$	0.8165	0.8165
EQPA, $M = 512$	0.4654	0.5350
kMC, $M = 512$	0.5235	0.5767
PM, $M = 512$	0.5894	0.6217
PA-PSK, $M = 512$	0.4419	0.4419

It is known in digital communications that a large minimum distance of a constellation results in a better error performance. In order to study these effects for PSKH, Fig. 2 shows the symbol error rate (SER) for constellations when 3 antennas are used with constellation sizes  $M = 64$  and  $M = 512$ . Fig. 2a shows transmission over a vector AWGN channel, i.e.,  $\mathbf{H} = \mathbf{I}$ . For Fig. 2b, every element of  $\mathbf{H}$  is a complex i.i.d. Gaussian random variable with unit variance. In both cases one can observe that the error performance of the constellation is ordered according to the minimum distance of the constellation. It is important to note that the minimum distance is not only a good measure for performance over the vector AWGN channel, but also if  $\mathbf{H}$  is a random matrix.

*Remark:* We note that PA-PSK with  $M = 64$  for 3 antennas is regular 4-PSK on each antenna. Without further modification, an optimized constellation such as PM can give a substantial gain compared to 4-PSK/antenna of almost 1.5 dB on the vector AWGN channel, which is equivalent to 3 subsequent transmissions over a regular AWGN channel. Such constellations which use a Single-Input Single-Output (SISO) channel multiple times are also known as multidimensional constellations [10]. So far, no work has dealt with multidimensional constellations with fixed radius. In [11], multidimensional QAM constellations were interpreted as a new form of diversity in order to combat fading.

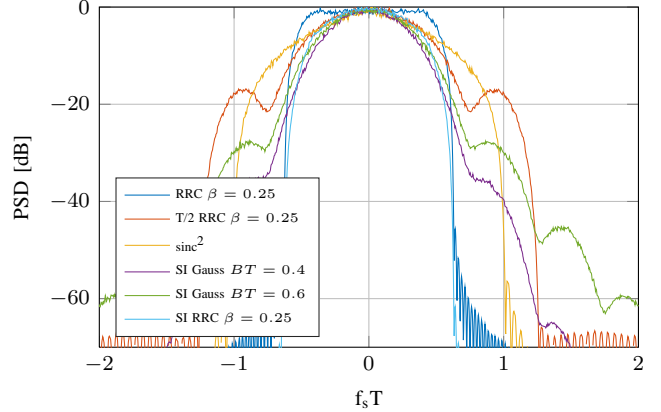


Fig. 3. Occupied spectra of different pulse shaping methods. The spectra are calculated for a  $n = 4$  antenna system.

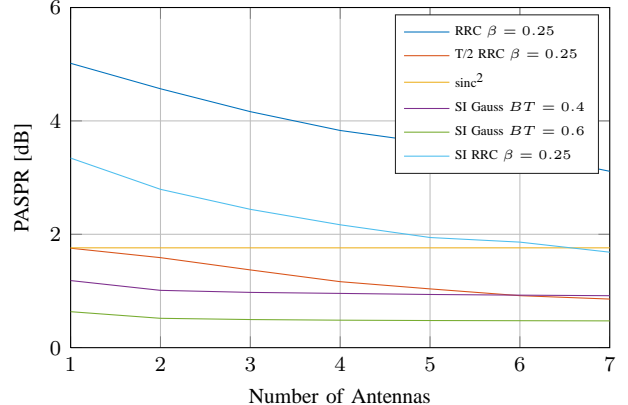


Fig. 4. Resulting PASPRs of different pulse shaping methods.

#### IV. PASPR AND SPECTRUM USAGE

In order to make full use of load-modulated MIMO transmitters, a constant energy constellation is only the first step. Further PASPR reduction techniques can be used in order to fully exploit load-modulation. Some methods may have a negative impact on the bandwidth. A wider spectrum may be

tolerable, if the gain in PASPR is substantial.

In this section, we present the spectrum and PASPR for three different PASPR reduction techniques and compare them with conventional intersymbol interference (ISI)-free PAM transmission. Our baseline is a root raised cosine (RRC) pulse shaping filter with roll-off factor  $\beta = 0.25$ . The comparison of spectra and PASPR is given in Figs. 3 and 4, respectively. In these plots, RRC and  $\text{sinc}^2$  describes conventional pulse shaping (see Sec. V for  $\text{sinc}^2$  pulse shaping), T/2-RRC describes pulse shaping at twice the symbol rate and SI RRC and SI Gauss is pulse shaping using spherical interpolation with a RRC or Gaussian filter (see Sec. VI).

The general result regarding bandwidth and PASPR is the following:  $\text{sinc}^2$  pulse shaping is the simplest way to reduce the PASPR at the cost of increased bandwidth. T/2-RRC and and SI Gaussian can reduce the PASPR even further, but a Gaussian pulse shaping filter has relatively high side lobes. SI RRC shows the least PASPR reduction, but it also reduces the occupied bandwidth slightly. A slightly better PASPR can be achieved by increasing the roll-off factor  $\beta$ .

A decisive factor for the bandwidth is the energy contained in a certain amount of bandwidth. In the remainder of this paper, we will use the 99.9%-bandwidth  $B_{99.9\%}$  of signals, i.e., the bandwidth that stores 99.9% of the signals' energy, to compare different pulse shaping methods. This is necessary to have a fair comparison, because noise power is proportional to the signal bandwidth. Due to high side lobes, Gaussian filters might suffer proportionally more when we increase  $B_{99.9\%}$  to  $B_{99.999\%}$ . We give additional information when appropriate.

In order to evaluate why Gaussian and  $\text{sinc}^2$  pulse shaping provide so much better PASPRs than a RRC even for one antenna, Appendix A and B provide some bounds and calculations on the PAPR of these pulse shapes. We show that the PAPR of  $\text{sinc}^2$  and Gaussian is close or equal to 1, whereas a sinc (which is closely related to RC and RRC) is generally unbounded.

## V. SINC<sup>2</sup> PULSE SHAPING

The simplest method from the ones presented in Sec. IV is to use a  $\text{sinc}^2(t)$ -function for pulse shaping. This means that the continuous transmission signal is

$$\mathbf{s}(t) = \sum_{k=-\infty}^{\infty} \mathbf{x}[k] * \text{sinc}^2\left(\frac{t - kT}{T}\right). \quad (7)$$

Here,  $*$  denotes elementwise convolution. Since  $\text{sinc}^2$  is not a  $\sqrt{\text{Nyquist}}$ -function, some ISI has to be equalized at the receiver. This ISI is not generated by the channel, but only by the pulse shaping filter and its corresponding matched filter, i.e., there is no ISI between different receive antennas. Thus there is no need to make use of equalization techniques developed for MIMO ISI channels. Instead, we filter the received signal of each antenna using Forney's *Whitened Matched Filter* (WMF) [12]. ISI can then be expressed by a one-dimensional, causal minimum-phase filter  $h_W[i]$  and the resulting discrete time transmission model becomes

$$\mathbf{y}[k] = \mathbf{H} \sum_{i=0}^L h_W[i] \mathbf{x}[k-i] + \mathbf{n}[k] \quad (8)$$

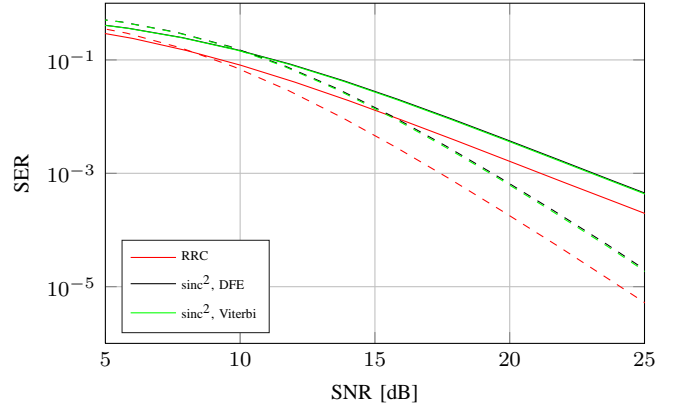


Fig. 5. Comparison of RRC and  $\text{sinc}^2$  pulse shaping. Transmission is over  $n = 2$  (solid) and  $n = 3$  (dashed) antennas with one bit per real dimension ( $M = 16$  and  $M = 64$ ).

with ISI-length  $L$ . ISI can be equalized with Maximum Likelihood Sequence Estimation (MLSE) using the Viterbi Algorithm (VA) [13] or Decision Feedback Equalization (DFE). In this specific case, almost all energy of  $h_W$  is stored in the very first coefficient  $h_W[0]$ , such that there is virtually no loss in terms of error probability.

Fig. 5 shows numerical results for  $\text{sinc}^2$  pulse shaping: DFE- and MLSE show the same performance, but in all cases they show a loss of 1.83 dB compared to the RRC. This is exactly the loss due to the wider spectrum which results in slightly more noise power. This gap grows up to 1.98 dB if one decides to use  $B_{99.999\%}$ . We note that despite this loss in bandwidth efficiency,  $\text{sinc}^2$  pulse shaping might still be a reasonable option for systems with very few antennas: In this case, the power saved by the reduced PASPR might make up for the loss in bandwidth efficiency.

## VI. SPHERICAL INTERPOLATION SIGNALING

Spherical interpolation signaling (SIS) tries to smoothen the transmission signal by forcing it onto the hypersphere also in-between data samples. This is achieved by inserting interpolation points at a certain oversampling rate. The positive effect is a significantly reduced PASPR compared to conventional PAM because the signal becomes smoother and deviations from the hypersphere are reduced, especially zero-crossings. The disadvantages are ISI introduced by the interpolation points and thus an increased receiver complexity.

Before presenting our two approaches, we define spherical interpolation also known as SLERP [14]: Given two points  $\mathbf{x}_1, \mathbf{x}_2 \in \mathbb{R}^N$  with  $\|\mathbf{x}_1\| = \|\mathbf{x}_2\| = 1$  and  $\cos(\theta) = \mathbf{x}_1 \cdot \mathbf{x}_2$ , for any  $0 \leq \tau \leq 1$ , the spherical interpolation of  $\mathbf{x}$  and  $\mathbf{y}$  is given as

$$\mathbf{SI}(\mathbf{x}_1, \mathbf{x}_2, \tau) = \frac{\sin((1-\tau)\theta)}{\sin \theta} \mathbf{x}_1 + \frac{\sin(\tau\theta)}{\sin \theta} \mathbf{x}_2. \quad (9)$$

### A. $\frac{T}{2}$ -Pulse Shaping

As mentioned, introducing spherical interpolation samples introduces ISI. In order to simplify equalization, our first approach is to generate ISI by means of an  $\sqrt{\text{Nyquist}}$ -filter.

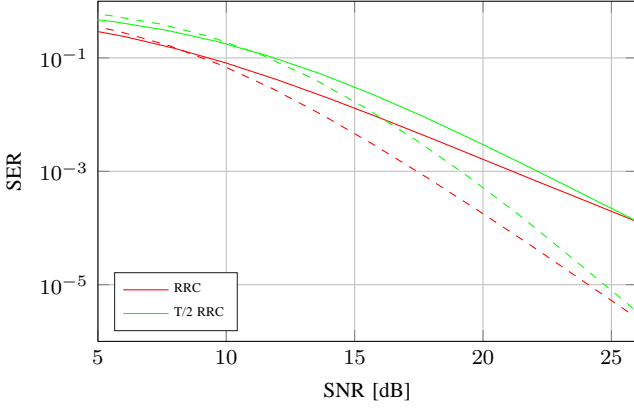


Fig. 6. Comparison of RRC and  $\frac{T}{2}$  pulse shaping. Transmission is over  $n = 2$  (solid) and  $n = 3$  (dashed) antennas with one bit per real dimension ( $M = 16$  and  $M = 64$ ).

This means we use a pulse shaping filter  $h(t)$  at twice the symbol rate. The resulting signal on antenna  $i$  is

$$\mathbf{s}(t) = \sum_{k=-\infty}^{\infty} \left( \mathbf{x}[k] * h(2(t - kT)) + \mathbf{SI} \left( \mathbf{x}[k], \mathbf{x}[k+1], \frac{1}{2} \right) * h \left( 2 \left( t - \left( k + \frac{1}{2} \right) T \right) \right) \right) \quad (10)$$

which is  $\sqrt{\text{Nyquist}}$  with respect to half the symbol rate. The corresponding matched filter is  $h^*(-2t)$ . Sampling with a rate of  $\frac{T}{2}$  gives a sequence of data points and interpolation values at the receiver.

To keep this system comparable with conventional PAM, both data and interpolation points contain only half the energy. Therefore it is necessary to use all points at the receiver to estimate the data sequence, otherwise half of the energy would be wasted. Data estimation for  $\frac{T}{2}$ -pulse shaping is done via the Viterbi algorithm.

It is obvious that this method has a huge disadvantage due to the much larger spectrum it occupies. The reason why we nevertheless include it in this comparison is that  $\frac{T}{2}$ -pulse shaping increases the slope of the error curve such that in the medium- to high-SNR regime it might still be a valid alternative given the largely reduced PASPR compared to conventional PAM. Results for this pulse shaping method are plotted in Fig. 6.

This increased slope can be explained by the linear transformation of the hypersphere induced by  $\mathbf{H}$ : At high SNRs, symbol errors will usually occur because the noise moves the data symbol into the decision region of a neighboring symbol. Symbol errors where the received symbol is in a decision region of a symbol from the opposite site of the hypersphere occur only rarely, because such points are farthest apart. If the receiver constellation  $\mathbf{H}\mathcal{A} = \{\mathbf{H}\mathbf{x} \mid \mathbf{x} \in \mathcal{A}\}$  is distorted enough, such errors may be much more likely because the distance between opposing points might be drastically reduced. In the case of  $\frac{T}{2}$ -pulse shaping, not only the distance between constellation points, but also the distance between interpolation points affects the performance of the system. For data points on

opposing sides of the hypersphere,  $\frac{T}{2}$ -pulse shaping generates interpolation points which are usually far away from each other. This increases the total minimum distance and thus the performance of the transmission. The magnitude of this effect is dependent on  $\mathbf{H}$ . A good measure for this effect is the ratio  $\frac{\sigma_{\text{SVD},\text{max}}}{\sigma_{\text{SVD},\text{min}}}$  with  $\sigma_{\text{SVD},\text{max}}$  and  $\sigma_{\text{SVD},\text{min}}$  being the maximum and minimum singular values of the real representation of  $\mathbf{H}$ , respectively<sup>2</sup>. The two extreme cases would be  $\frac{\sigma_{\text{SVD},\text{max}}}{\sigma_{\text{SVD},\text{min}}} = 1$  in which  $\mathbf{H}\mathcal{A}$  would still be a hypersphere (possibly with a different radius) and  $\frac{\sigma_{\text{SVD},\text{max}}}{\sigma_{\text{SVD},\text{min}}} \rightarrow \infty$ . In the latter case, the  $n$ -dimensional hypersphere would be compressed down to fewer dimensions, effectively making opposing constellation points neighboring points.

### B. Spherical Interpolation

The main problem of  $\frac{T}{2}$ -pulse shaping is the large bandwidth due to the use of pulse shaping filters at higher frequency. In order to mitigate the problem, we combine spherical interpolation values with a conventional pulse shaping filter at its original frequency.

This method is characterized by the interpolation frequency  $f_{\text{IP}}$ , which determines how many signal points are transmitted in one symbol interval. This leads to the transmission signal

$$\mathbf{s}(t) = \sum_{k=-\infty}^{\infty} \left( \mathbf{x}[k] * h(t - kT) + \sum_{l=1}^{f_{\text{IP}}-1} \mathbf{SI} \left( \mathbf{x}[k], \mathbf{x}[k+1], \frac{l}{f_{\text{IP}}} \right) * h \left( t - \left( k + \frac{l}{f_{\text{IP}}} \right) T \right) \right). \quad (11)$$

At the receiver, we filter with the matched filter  $h^*(-t)$  followed by  $T$ -spaced sampling. Introducing the autocorrelation  $\rho(\tau) = \int_{-\infty}^{\infty} h(t+\tau)h^*(t)dt$ , the received discrete time signal is

$$\mathbf{y}[k] = \mathbf{y}(kT) = \mathbf{H} \left( \sum_{\bar{k}=-\infty}^{\infty} \mathbf{x}[\bar{k}] \rho(kT - \bar{k}T) + \sum_{l=1}^{f_{\text{IP}}-1} \mathbf{SI} \left( \mathbf{x}[\bar{k}], \mathbf{x}[\bar{k}+1], \frac{l}{f_{\text{IP}}} \right) \cdot \rho \left( kT - \left( \bar{k} + \frac{l}{f_{\text{IP}}} \right) T \right) \right) + \mathbf{n}[k]. \quad (12)$$

By using a  $\sqrt{\text{Nyquist}}$ -pulse, the direct influence of adjacent symbols may be suppressed (and the resulting noise at the receiver will be white), but the influence of the interpolation values remains. Thus ISI-equalization in form of MLSE via the VA is performed at the receiver. Fig. 7 shows the system model used at the receiver to estimate the data sequence. In order to do so, the VA has to be adapted in such a way that all  $f_{\text{IP}}$  vectors, which were transmitted during one symbol interval, are used to calculate the metric. Since  $T$ -spaced sampling is used, it is vital to use the contribution from the interpolation

<sup>2</sup>Every complex-valued model  $\mathbf{y} = \mathbf{H}\mathbf{x} + \mathbf{n}$  of dimension  $n$  can be transformed into an equivalent real-valued model of dimension  $2n$ , see e.g. [15].

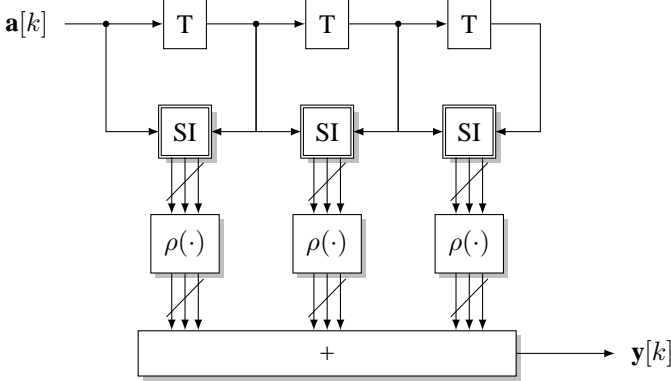


Fig. 7. System used to model the ISI produced by spherical interpolation transmission. An SI block calculates  $f_{IP}$  vectors and  $\rho(\cdot)$  weighs them with the autocorrelation of the pulse shaping filter. Thus each block processes all interpolation vectors within one symbol period. This model omits the channel matrix  $\mathbf{H}$  and noise  $\mathbf{n}$ .

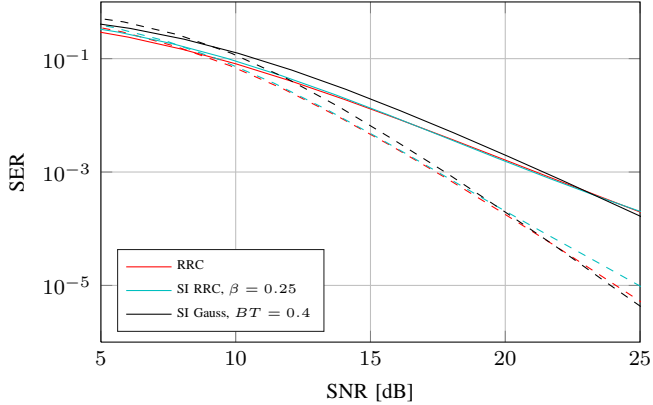


Fig. 8. Comparison of RRC and SI pulse shaping with  $f_{IP} = 4$ . Transmission is over  $n = 2$  (solid) and  $n = 3$  (dashed) antennas with one bit per real dimension ( $M = 16$  and  $M = 64$ ). The receiver used a Viterbi decoder with  $\nu = 2$  memory elements for  $n = 3$  antennas and  $\nu = 3$  memory elements for  $n = 2$  antennas.

values, otherwise their energy would be wasted. As a result, the system would not be competitive.

The choice of  $f_{IP}$  provides a trade-off between receiver complexity and smoothness of the output signal (which in turn improves PASPR and bandwidth). The results in Figs. 4 and 3 were generated using  $f_{IP} = 4$ . Increasing  $f_{IP}$  to 16 showed a 0.15 dB improvement in PASPR for a RRC and a 0.05 dB improvement for a Gaussian pulse shaping filter. The error probability is unaffected by increasing  $f_{IP}$ .

Fig. 8 shows numerical results for the spherical interpolation shaping using  $f_{IP} = 4$  with two different pulse shaping filters. Detection was performed using the VA employing  $\nu = 3$  memory elements for the 16-ary constellation and  $\nu = 2$  memory elements for the 64-ary constellation (corresponding to 4096 states in both cases). Since such a huge number of states is hard to implement in practice, we discuss some complexity reduction techniques and effects in the next section. Remaining pulse energy was equalized using DFE, which makes the overall scheme a Delayed Decision-Feedback Sequence Estimation (DDFSE) [16]. For DDFSE, usually

a prefilter is applied to make the overall impulse response minimum-phase, see e.g. [17]. In the case of both RRC and Gaussian filtering, we found that the minimum phase part of these filters has its energy spread over a much wider interval, which would require more memory elements in the VA to capture the same amount of energy. This is computationally not feasible. It is thus advantageous to use the original filter instead of applying any prefilter to make the overall filter minimum phase.

The results of the SI pulse shaping are extremely good: The performance is equivalent to conventional PSKH, but a large gain in PASPR is achieved by using this method. If RRC pulse shaping is applied to both SI and conventional PSKH, both methods have almost the same bandwidth. We thus trade power efficiency (reduced PASPR) for receiver complexity (DDFSE detection).

In the case of Gaussian pulse shaping, the spectral widening can become a problem: In the case of  $B_{99.9\%}$ , the required spectrum is only slightly wider. If we require  $B_{99.999\%}$  to be used, the performance of Gaussian pulse shaping with  $BT = 0.4$  degrades around 2.2 dB due to the increased noise power. This is because of the high sidelobes of the Gaussian filter.

### C. Complexity Reduction Techniques

As shown in Fig. 7, ISI needs to be equalized using the VA when spherical interpolation is used. It is usually sufficient to use only 2 or 3 delay elements to capture almost all energy of the pulse, the remaining energy at the end of the filter can be equalized by means of DDFSE. But since each delay element is  $M$ -ary, the number of states can become infeasible even for such a small number of elements. We thus compare system performance and complexity when using two different complexity reduction techniques: The well-known Reduced State Sequence Estimation (RSSE) [18] and an iterative application of the VA.

For RSSE, we use a Viterbi algorithm with  $\nu = 2$  memory elements and generate hypersymbols by using hypersymbols in the second delay element only. Combining different input symbols into a hypersymbol in the first element leads to large performance degradation due to two effects: Hypersymbols are calculated in advance based on the original constellation  $\mathcal{A}$ . We did this by numerically optimizing the minimum distance within each hypersymbol. The effective constellation at the receiver, however, is  $\mathbf{H}\mathcal{A}$  which might have a drastically different distance profile than the constellation with originally optimal hypersymbols. The other negative impact is the fact that both the impulse response  $\rho(t)$  as well as its minimum-phase do not have monotonously decreasing values. The decision in the first delay element is thus based on only a small fraction of the total pulse energy.

Our second approach to reduce the complexity is to apply the Viterbi algorithm iteratively. This works well if the performance gap between the use of  $\nu$  and  $\nu+1$  memory elements is not too large. The idea behind it is that if each error pattern is a neighboring symbol of the correct signal point, it is sufficient to consider these neighboring symbols in future steps. This is a valid assumption if the SNR is sufficiently high. Our algorithm works as follows:

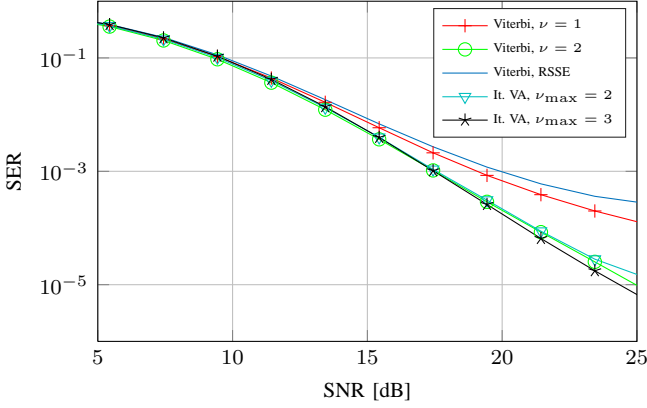


Fig. 9. Comparison of SI pulse shaping for  $n = 3$  antennas with a RRC pulse shape with  $\beta = 0.25$ . RSSE used a quaternary second delay element and  $n_{\text{NB}} = 4$  for all iterative variants.

TABLE II  
COMPLEXITY COMPARISON OF SI DEMODULATION

Algorithm	$\Xi$
Viterbi, $\nu = 1$	4096
Viterbi, $\nu = 2$	262144
Viterbi, RSSE	16384
It. Viterbi, $\nu_{\text{max}} = 2$	4221
It. Viterbi, $\nu_{\text{max}} = 3$	4721

- 1) Initialize  $\nu = 1$ .
- 2) Run the Viterbi algorithm with one memory element.
- 3) For each estimate  $\hat{\mathbf{x}}[k]$ , find the  $n_{\text{NB}}$  nearest neighboring points.
- 4) Set  $\nu = \nu + 1$ .
- 5) Run the Viterbi algorithm with  $\nu$  memory elements, only allowing  $n_{\text{NB}} + 1$  points in each time step.
- 6) If  $\nu = \nu_{\text{max}}$  finish, otherwise go back to 2.

The neighboring points can be calculated in advance and stored in a table. This works best if the neighboring points are taken from  $\mathbf{H}\mathcal{A}$ , but a reasonable performance can also be achieved if they are taken directly from  $\mathcal{A}$ , which reduces the overhead to recalculate them every time  $\mathbf{H}$  changes.

Fig. 9 shows the performance for a RRC with  $\beta = 0.25$  and transmission over three antennas. The VA curve using two memory elements ( $\nu = 2$ ) is the same as in Fig. 8 and is our baseline. As a measure of complexity we count the number of branches in each time step

$$\Xi = \begin{cases} M^{\nu+1}, & \text{Standard VA} \\ M \cdot \prod_{i=1}^{\nu} M_i, & \text{VA, RSSE} \\ M^2 + \sum_{i=2}^{\nu_{\text{max}}} (n_{\text{NB},i} + 1)^{\nu_i+1}, & \text{Iterative VA.} \end{cases} \quad (13)$$

In this term,  $M_i$  is the number of possible values in the  $i$ -th delay element if RSSE is used (the number of hypersymbols) and  $\nu_i$  is the number of memory elements in the  $i$ -th iteration of the iterative VA. Table II shows the complexity for the algorithms used to create Fig. 9. As one can see, the iterative Viterbi provides the best performance with only minor increase compared to the VA which uses only one memory element.

It should be noted, however, that the exact performance of

the complexity reduction techniques is dependent on the pulse shaping filter. In the case of Gaussian pulse shaping, only a small improvement can be seen from  $\nu = 1$  to  $\nu = 3$  with both iterative VA and RSSA VA showing similar results. For the sake of brevity, we omit further plots and an extended discussion for the Gaussian case.

## VII. CONCLUSION

We introduced PSKH and discussed different methods to generate data constellations on the hypersphere and their performance. We then discussed various methods of pulse shaping in order to reduce the PASPR of the signals, which allows an efficient use of load-modulation amplifiers. These different methods provide a trade-off between power efficiency, spectral efficiency and receiver complexity. It is possible to reduce the PASPR without sacrificing spectral efficiency, thus proving that load-modulation amplifiers are a valid approach not only for massive MIMO systems, but also if only a small number of antennas is employed.

## APPENDIX A

### PAPR OF SIGNALS USING sinc AND sinc<sup>2</sup> PULSE SHAPING

*Theorem 1:* W.l.o.g. assume that an alphabet  $\mathcal{A} = \{a_0, \dots, a_{M-1}\}$ ,  $a_i \in \mathbb{R}$  with  $\max_i |a_i| = 1$  is given and an arbitrary data sequence with symbol rate  $1/T$  is used to generate a continuous signal

$$g(t) = \sum_{k=-\infty}^{\infty} a[k] * \text{sinc}\left(\frac{t - kT}{T}\right) \quad (14)$$

with  $a[k] \in \mathcal{A}$ . Then  $\max_t |g(t)|^2 = \infty$ .

*Proof:* W.l.o.g. we set  $T = 1$  and maximize  $|g(t)|$  instead of  $|g(t)|^2$ , which is achieved at the same point.  $\text{sinc}(t)$  has no sign changes in an interval  $(k, k+1)$  for  $k \in \mathbb{Z}$ , thus  $g(t)$  is maximized if all superimposed sinc functions have the same sign in a given interval and a coefficient with maximum amplitude. In the interval  $[0, 1]$ , this is achieved if we choose  $a[k] = -1$  if  $k$  is even and positive or odd and negative. Otherwise, we choose  $a[k] = 1$ . This gives

$$g(t) = \text{sinc}(t) + \sum_{k=1}^{\infty} (-1)^{k+1} \text{sinc}(t - k) + \sum_{k=-\infty}^{-1} (-1)^k \text{sinc}(t - k) \quad (15)$$

which is symmetric around  $\frac{1}{2}$ .

In order to find the maximum of  $g(t)$ , we can split the function into all pulses right of the symmetry axis and all those left of the axis. This gives us

$$g_1(t) = \sum_{k=-\infty}^{-1} (-1)^k \text{sinc}(t - k) + \text{sinc}(t) \quad (16)$$

$$g_2(t) = \sum_{k=1}^{\infty} (-1)^{k+1} \text{sinc}(t - k). \quad (17)$$

Note that due to symmetry, for  $0 \leq t \leq 1$  we have  $g_1(t) = g_2(1-t)$  and  $g_1(1-t) = g_2(t)$ . This allows to express the derivative as

$$\begin{aligned} g'(t) &= (g_1(t) + g_2(t))' = (g_1(t) + g_1(1-t))' \\ &= g_1'(t) - g_1'(1-t) \end{aligned} \quad (18)$$

which is zero for  $g_1'(t) = g_1'(1-t)$ . This is obviously fulfilled for  $t = \frac{1}{2}$ . In fact,  $t = \frac{1}{2}$  is the only extremal value in the interval  $(0, 1)$ . This can be proven by looking at the monotonicity and concavity of each sinc pulse around its local maximum in this interval. We omit this part for the sake of brevity.

Because of  $2\text{sinc}(\frac{1}{2}) > 1$  we can conclude that there is no maximum at the boundary of our interval. We already chose  $|a[k]| = 1$ , thus the extremal value is

$$\max |g(t)| = \sum_{k=-\infty}^{\infty} \left| \text{sinc}\left(\frac{1}{2} - k\right) \right|. \quad (19)$$

In order to proof divergence of this value, we rewrite

$$\begin{aligned} \left| \text{sinc}\left(\frac{1}{2} - k\right) \right| &= \left| \frac{\sin(\pi(\frac{1}{2} - k))}{\pi(\frac{1}{2} - k)} \right| \\ &= \left| \frac{\cos(\pi k)}{\pi(\frac{1}{2} - k)} \right| = \frac{1}{|\pi(\frac{1}{2} - k)|}. \end{aligned} \quad (20)$$

We can thus rewrite the maximum as

$$\sum_{k=-\infty}^{\infty} \left| \text{sinc}\left(\frac{1}{2} - k\right) \right| = 2\text{sinc}\left(\frac{1}{2}\right) + \frac{2}{\pi} \sum_{k=2}^{\infty} \frac{1}{k - \frac{1}{2}} \quad (21)$$

which is essentially a harmonic series which is known to diverge.  $\blacksquare$

*Theorem 2:* Using the same assumptions as in Theorem 1, a continuous signal is generated as

$$g(t) = \sum_{k=-\infty}^{\infty} a[k] * \text{sinc}^2\left(\frac{t - kT}{T}\right). \quad (22)$$

Then  $\max_t |g(t)|^2 = 1$ .

*Proof:* W.l.o.g., we assume  $T = 1$  again. The proof's first steps are the same as above, but in this case we set  $a[k] = 1 \forall k$  because  $\text{sinc}^2$  is nonnegative for all input values. Because of  $2\text{sinc}^2(\frac{1}{2}) < 1$ , the maximum is either at  $t = 0$  or  $t = \frac{1}{2}$ . We know that  $g(0) = 1$ , so we take a closer look at  $t = \frac{1}{2}$ . Following the steps above gives us

$$\text{sinc}^2\left(\frac{1}{2} - k\right) = \frac{1}{\pi^2} \frac{1}{(\frac{1}{2} - k)^2} \quad (23)$$

which we can use to rewrite

$$\begin{aligned} g\left(\frac{1}{2}\right) &= \sum_{k=-\infty}^{\infty} \text{sinc}^2\left(\frac{1}{2} - k\right) \\ &= 2\text{sinc}^2\left(\frac{1}{2}\right) + \frac{2}{\pi^2} \sum_{k=2}^{\infty} \frac{1}{(\frac{1}{2} - k)^2}. \end{aligned} \quad (24)$$

Evaluating the sum-term using [19, p.9, eq. 0.234-2] gives

$$\sum_{k=2}^{\infty} \frac{1}{(\frac{1}{2} - k)^2} = 4 \cdot \left( \sum_{k=0}^{\infty} \frac{1}{(2k-1)^2} - 2 \right) = \frac{1}{2}(8 + \pi^2) - 8. \quad (25)$$

We can now use  $\text{sinc}^2\left(\frac{1}{2}\right) = \frac{4}{\pi^2}$  and insert it together with eq. (25) into eq. (24) to get

$$\sum_{k=-\infty}^{\infty} \text{sinc}^2\left(\frac{1}{2} - k\right) = 2 \cdot \frac{4}{\pi^2} + \frac{2}{\pi^2} \cdot \left( \frac{1}{2}(8 + \pi^2) - 8 \right) = 1 \quad (26)$$

■

## APPENDIX B PAPR OF SIGNALS USING GAUSSIAN PULSE SHAPING

*Theorem 3:* Using the same assumptions as in Theorem 1, a continuous signal is generated as

$$g(t) = \sum_{k=-\infty}^{\infty} a[k] * \exp\left(-\left(\frac{\pi}{\alpha}(t - kT)\right)^2\right) \quad (27)$$

with  $\alpha = \frac{\sqrt{\ln(2)}}{\sqrt{2}B}$ . Then  $\max_t |g(t)|^2 < \infty$  and  $\lim_{B \rightarrow \infty} \max_t |g(t)|^2 = 1$  with  $\max_t |g(t)|^2$  monotonously decreasing in B.

*Proof:* W.l.o.g. we assume  $T = 1$  and introduce  $\gamma = \frac{2\pi^2 B^2}{\ln(2)}$ . With  $\exp(-x^2) > 0 \ \forall x \in \mathbb{R}$  the maximum is achieved by choosing  $a[k] = 1 \ \forall k$ . We thus have

$$g(t) = \sum_{k=-\infty}^{\infty} \exp\left(-\gamma(t - k)^2\right). \quad (28)$$

By means of the ratio test it is easy to show that this sum converges for all  $t$ . Thus  $\max_t |g(t)| < \infty$  from which we can conclude that  $\max_t |g(t)|^2 < \infty$ .

In order to find where the maximum is achieved, we take the derivative

$$g'(t) = \sum_{k=-\infty}^{\infty} 2\gamma \exp\left(-\gamma(t - k)^2\right) (k - t) \quad (29)$$

and note that there is point symmetry at each integer value of  $t$ . Each term of the sum vanishes at  $t = k$ , but because of the symmetry the sum of all remaining terms is zero as well. Thus we have  $g'(t) = 0 \ \forall t \in \mathbb{Z}$ . Choosing  $t = 0$  yields

$$\max g(t) = \sum_{k=-\infty}^{\infty} \exp(-\gamma k^2). \quad (30)$$

Because  $\lim_{B \rightarrow \infty} \exp(-\gamma k^2) = 0 \ \forall k \neq 0$  we get  $\lim_{B \rightarrow \infty} \max_t |g(t)|^2 = 1$ .  $\blacksquare$

Note that even for practical values of  $B$ , the maximum of  $g(t)$  is only slightly larger than 1, e.g.,  $\max g(t) \approx 1.15$  for  $B = 0.3$ .

## REFERENCES

- [1] F. H. Raab, P. Asbeck, S. Cripps, P. B. Kenington, Z. B. Popovic, N. Pothecary, J. F. Sevic, and N. O. Sokal, "RF and Microwave Power Amplifier and Transmitter Technologies - Part 1," *High Frequency Electronics*, vol. 2, no. 3, pp. 22–36, 2003.
- [2] M. A. Sedaghat, R. R. Müller, and G. Fischer, "A Novel Single-RF Transmitter for Massive MIMO," in *Proc. ITG Workshop on Smart Antennas*, 2015.
- [3] R. R. Müller, M. A. Sedaghat, and G. Fischer, "Load Modulated Massive MIMO," in *Proc. of IEEE Global Conference on Signal and Information Processing*, 2014.
- [4] M. A. Sedaghat, R. R. Müller, and C. Rachinger, "(Continuous) Phase Modulation on the Hypersphere," *IEEE Transactions on Wireless Communications*, vol. PP, no. 16, May 2016.
- [5] J. H. Conway and N. J. A. Sloane, *Sphere Packing, Lattices and Groups*. Springer, 1998.
- [6] N. J. A. Sloane, R. H. Hardin, W. D. Smith *et al.* Tables of Spherical Codes. [Online]. Available: <http://neilsloane.com/packings/>
- [7] P. Leopardi, "A partition of the unit sphere into regions of equal area and small diameter," *Electronic Transactions on Numerical Analysis*, vol. 25, pp. 309–327, 2006.
- [8] I. S. Dhillon and D. S. Modha, "Concept Decompositions for Large Sparse Text Data Using Clustering," *Machine Learning*, vol. 42, no. 1, pp. 143–175, January 2001.
- [9] J. M. Haile, *Molecular Dynamics Simulation: Elementary Methods*. Wiley, 1997.
- [10] G. D. Forney and L.-F. Wei, "Multidimensional Constellations - Part I: Introduction, Figures of Merit, and Generalized Cross Constellations," *IEEE Journal on Selected Areas in Communications*, vol. 7, no. 6, pp. 877–892, August 1989.
- [11] J. Boutros and E. Viterbo, "Signal Space Diversity: A Power- and Bandwidth-Efficient Diversity Technique for the Rayleigh Fading Channel," *IEEE Transactions on Information Theory*, vol. 44, no. 4, pp. 1453–1467, July 1998.
- [12] G. D. Forney, "Maximum-likelihood sequence estimation of digital sequences in the presence of intersymbol interference," *IEEE Transactions on Information Theory*, vol. 18, no. 3, pp. 363–378, May 1972.
- [13] A. Viterbi, "Error Bounds for Convolutional Codes and an Asymptotically Optimum Decoding Algorithm," *IEEE Transactions on Information Theory*, vol. 13, no. 2, pp. 260–269, April 1967.
- [14] K. Shoemake, "Animating Rotation with Quaternion Curves," in *Proc. 12th Annual Conference on Computer Graphics and Interactive Techniques (SIGGRAPH)*, San Francisco, USA, July 1985, pp. 245–254.
- [15] I. E. Telatar, "Capacity of Multi-antenna Gaussian Channels," *European Transactions on Telecommunications*, vol. 10, no. 6, pp. 585–595, 1999.
- [16] A. Duel-Hallen and C. Heegards, "Delayed Decision-Feedback Sequence Estimation," *IEEE Transactions on Communications*, vol. 37, no. 5, pp. 428–436, May 1989.
- [17] W. H. Gerstacker, F. Obernosterer, R. Meyer, and J. B. Huber, "An Efficient Method for Prefilter Computation for Reduced-State Equalization," in *Proc. IEEE International Symposium on Personal, Indoor and Mobile Radio Communication (PIMRC)*, London, September 2000, pp. 604–609.
- [18] M. V. Eyuboglu and S. U. H. Qureshi, "Reduced-State Sequence Estimation with Set Partitioning and Decision Feedback," *IEEE Transactions on Communications*, vol. 36, no. 1, pp. 13–20, January 1988.
- [19] I. Gradshteyn and I. Ryzhik, *Table of Integrals, Series, and Products*, 7th ed., A. Jeffrey and D. Zwillinger, Eds. Elsevier, 2007.